Second International Symposium on Marine Propulsors
smp'11, Hamburg, Germany, June 2011
Workshop: Propeller performance

Numerical Predictions of the Cavitating and Non-Cavitating Flow around the Model Scale Propeller PPTC

Mitja Morgut[1], Enrico Nobile[1]

[1]Dipartimento di Ingegneria Meccanica e Navale, University of Trieste, Trieste, Italy

ABSTRACT

In this work we simulate the non-cavitating and cavitating flow around the PPTC (Potsdam Propeller Test Case) model scale propeller. The calculations are carried out using the commercial CFD solver ANSYS CFX 12, and for the prediction of the cavitating behaviour three different mass transfer models, previously calibrated, are employed.

Keywords

UniTS, propeller, performance, calibration

1 INTRODUCTION

In this work we investigated the flow around the PPTC model scale propeller. Both cavitating and non-cavitating flow conditions were numerically analyzed. Two different geometries were used to carry out the *Towing tank test* analysis and the *Cavitation tunnel test* analysis, respectively. All the simulations were carried out using the ANSYS-CFX 12 (which will be referred to from now on as CFX) commercial CFD solver, and the cavitating flow predictions were carried out using three different mass transfer models. In particular we used the Zwart et al (2004) model, and the models inspired by the works of Kunz et al (2000) and Singhal et al (2002), which were previously properly tuned by means of an optimization strategy (Morgut et al 2011, Morgut & Nobile 2011). Moreover we would like to mention that at the moment work is in progress in order to obtain accurate results also using the OpenFOAM OpenSource CFD library.

In the following we present first the propeller model, followed by the report on the numerical simulation regarding *Towing tank tests*. Then, the description of the numerical simulations carried out for the *Cavitation tunnel tests* is provided.

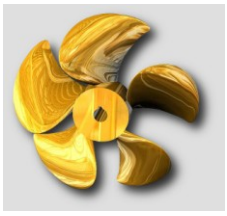

Figure 1: PPTC propeller model

2 PROPELLER MODEL

In this study we considered the propeller PTTC visible in Figure 1. It is a model scale, five bladed controllable pitch propeller with a diameter D=250mm. The experimental datasets cover the open water characteristics, velocity field measurements and cavitation tests.

3 TOWING TANK TESTS

3.1 Numerical Strategy

Since in the open-water tests the propeller moves forward in a homogeneous uniform flow, taking advantage of the periodicity of the problem we carried out the numerical simulations considering only one blade passage. The propeller rotation was simulated using the MRF (Multiple Reference Frame) approach. Thus the computational domain, defined as a segment of a cylinder covering only one blade passage, was subdivided into a rotating part, named *Rotating*, and stationary part, called *Fixed*, as illustrated in Figure 2. The front and aft boundaries (interfaces) delimiting *Rotating* were placed 0.7D and 0.6D from the propeller mid plane, respectively. The top boundary was placed at a radius of 0.6D from the rotation axis centreline. For *Fixed* the Inlet and Outlet boundaries were places 2.3D and 5.3D from the propeller mid plane, while the Top boundary was placed at a radius of 5D from the rotation axis centreline.

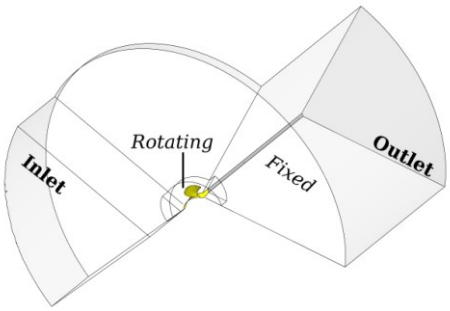

Figure 2: Computational domain for the Towing tank tests

In order to reproduce numerically the *Towing tank tests* the following boundary conditions were used. On the Inlet boundary a turbulence intensity of 1% and the free stream velocity in the axial direction V were set. Since in all the simulations the rotational velocity of the propeller was kept fix to n=15rps, the value of velocity V on the Inlet

boundary was varied accordingly to the values of the advance coefficient, $J=V/nD$. On the Outlet boundary a fixed value of static pressure was imposed. On the periodic boundaries (sides of the domain) the rotational periodicity was ensured. On all solid surfaces the no slip boundary condition was applied, and on the Top boundary of the domain the slip condition was imposed. For turbulence closure the two equation Shear Stress Transport SST turbulence model in combination with the automatic wall treatment was employed (Menter 1998).

3.2 Meshing

In this case both the parts, i.e. *Rotating* and *Fixed*, were discretized independently, with ANSYS-ICEM 12, using the hybrid meshing approach and joined in CFX using the GGI (Generalized Grid Interface) capability of the solver. In particular for both parts we first generated the surface and volume meshes using the robust OCTREE model (ANSYS, 2006). Then in order to resolve the turbulent boundary layer we placed four layers of prisms on the portion of hub belonging to *Fixed* and eight layers of prisms on the portion of hub belonging to *Rotating*. Eight layers of prisms were placed also around the blade surface. For *Fixed* we generated only one mesh having 65439 nodes. On the other hand for *Rotating* we generated two meshes with different resolution. The default one with 370659 nodes and the finer one with 586057 nodes. In Figure 3 we present the blade surface mesh for the default (coarser) mesh.

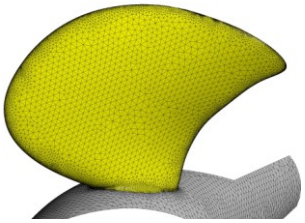

Figure 3: Hybrid blade surface mesh

Moreover, the meshes were generated in order to guarantee almost the same average value of y^+ on the solid surfaces of blade and hub of about 30 and 18 for J=1, respectively.We remind that y^+ is defined as $y^+ = \mu_\tau y / \nu$, where $\mu_\tau = (\tau_w / \rho_l)^{1/2}$ is the friction velocity, y the normal distance from the wall, ν the kinematic viscosity, ρ_l the liquid density and τ_w the wall shear stress.

3.3 Propeller performances

Figure 4 shows that the propeller performances predicted with the different resolution meshes were very close to each other. For the thrust coefficient K_T the differences were less than 1.5% whereas for the torque coefficient K_Q the differences were less than 2.5%. K_T and K_Q were defined as:

$$K_T = \frac{T}{\rho_l n^2 D^4} \qquad K_Q = \frac{Q}{\rho_l n^2 D^5} \tag{1}$$

where T (N) was the thrust, Q (Nm) the torque, ρ_l water density.

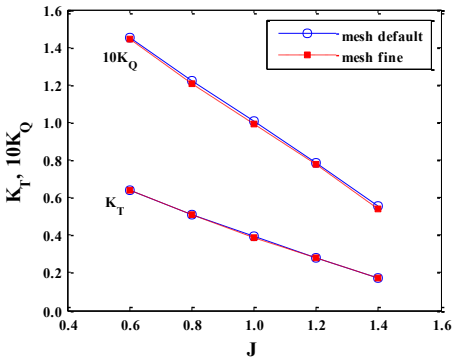

Figure 4: Propeller performances (non-cavitating)

4 CAVITATION TUNNEL TESTS

4.1 Numerical Strategy

Analogously to the simulations relative to the *Towing tank tests*, also for the *Cavitation tunnel tests* we simulated the propeller flow with the MRF approach considering only one blade passage. However in this case for *Fixed* we used, inspired by Müller et al (2009), a simpler shape, as illustrated in Figure 5. The domain has the following dimensions. The front and aft boundaries (interfaces) delimiting *Rotating* were placed 0.41D and 0.31D from the propeller mid plane, respectively. The top boundary has a radius of 0.6D from the rotation axis centreline. For *Fixed* the Inlet and Outlet boundaries were placed 2.3D and 5.3D from the propeller mid plane, while the top boundary was placed 5D from the rotation axis centreline.

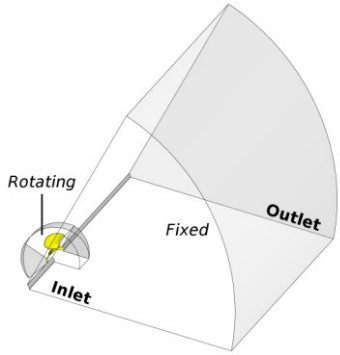

Figure 5: Computational Domain for Cavitation Tunnel Test

The non cavitating flow was simulated following the numerical setup for the *Towing tank tests*, while, for the cavitating flow investigations an additional modelling was required, in order to evaluate the mass transfer rate between vapour and water phases. In order to model the mass transfer between the two different phases we used three different mass transfer models. We used the Zwart et al (2004) model, the model inspired by the work of Kunz et al (2000) and the model proposed by Singhal et al (2002) also known as Full Cavitation Model (for brevity FCM). Moreover we point out that in order to improve the accuracy of the numerical predictions all the models were previously calibrated using an optimization strategy (Morgut & Nobile 2011).

The different cavitating flow regimes, determined by the cavitation number, σ_n, were defined varying the value of

the saturation pressure P_v. This is because P_{ref} , ρ_l were kept constant and σ_n was defined, in this case, as:

$$\sigma_n = \frac{P_{ref} - P_v}{0.5\rho_l (nD)^2} \qquad (2)$$

where $P_{ref}=P_{outlet,}$ and n (rps) was the rotational speed of the propeller.

4.2 Meshing

Also in this case the meshes were generated with ANSYS ICEM 12. Both parts of the domain, i.e. *Rotating* and *Fixed*, were discretized independently by hexahedral meshes and then joined in CFX using GGI capability of the solver. For *Fixed* we used always the same mesh having 275680 nodes. For *Rotating* instead we generated three progressively finer meshes, i.e. mesh A with 889146 nodes, mesh B with 1838655 nodes and mesh C with 2360214 nodes. We specify that mesh B was generated from mesh A increasing the node distributions along the edges by a factor of 1.25, whereas the mesh C was generated from mesh B increasing the mesh resolution in the tip vortex region. Moreover al the three different meshes had the same distance of the first node from the solid surfaces leading to the average value of y^+=32 on solid surfaces, for J=1.253. For illustration purposes Figure 6 shows the blade surface discretization for the mesh A.

Figure 6: Hexa-structured blade surface mesh

4.3 Non-Cavitating Velocity Field

In this case the simulation was carried out for J=1.253 with the free-stream velocity assumed equal to V=7.204 m/s and rotational speed of the propeller equal to n=23 rps. The water density was fixed as ρ=997.1 kg/m^3 with a kinematic viscosity ν=0.903E-6 m^2/s. In Table 1 the values of the thrust $K_{T,NUM}$ and torque $K_{Q,\,NUM}$ coefficients computed with different meshes are presented.

Table 1:Thrust and Torque coefficients for J=1.253 (non-cavitating conditions)

Mesh	$K_{T,\,NUM}$	$10K_{Q,\,NUM}$
A	0.2497	0.719
B	0.2495	0.716
C	0.2496	0.716

From the results collected in Table 1 it is possible to point out that the numerical values of the thrust and torque coefficients, $K_{T,NUM,}$, $K_{Q,NUM}$ differed less than 2% of the experimental ones $K_{T,EXP}$ = 0.250, $10K_{Q,EXP}$ = 0.725.

In the following we present the velocity profiles, given in the stationary frame of reference, computed at r/R=1 for x/D=0.1 and x/D=0.2 respectively, where r was the radial distance from the rotation axis centreline, R the radius of the propeller and x the axial distance from the propeller mid plane in downstream direction.

For the sake of clarity we remind that the rotational angle was assumed positive in the clockwise direction (looking the propeller in upstream direction) with the zero angle corresponding to the 12 o'clock position of the propeller's blade. Moreover the axial velocities were assumed positive in the flow directions, radial velocities positive for increasing radii and tangential velocities positive in direction of the propeller rotation.

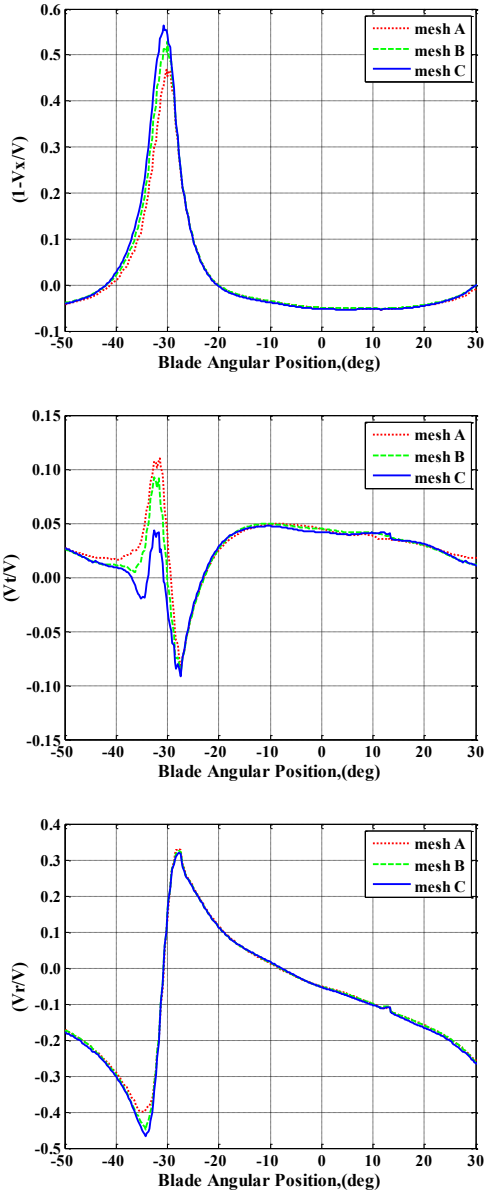

Figure 7: Velocity profiles computed in a plane x/D=0.1 downstream of the propeller mid plane at r/R=1.

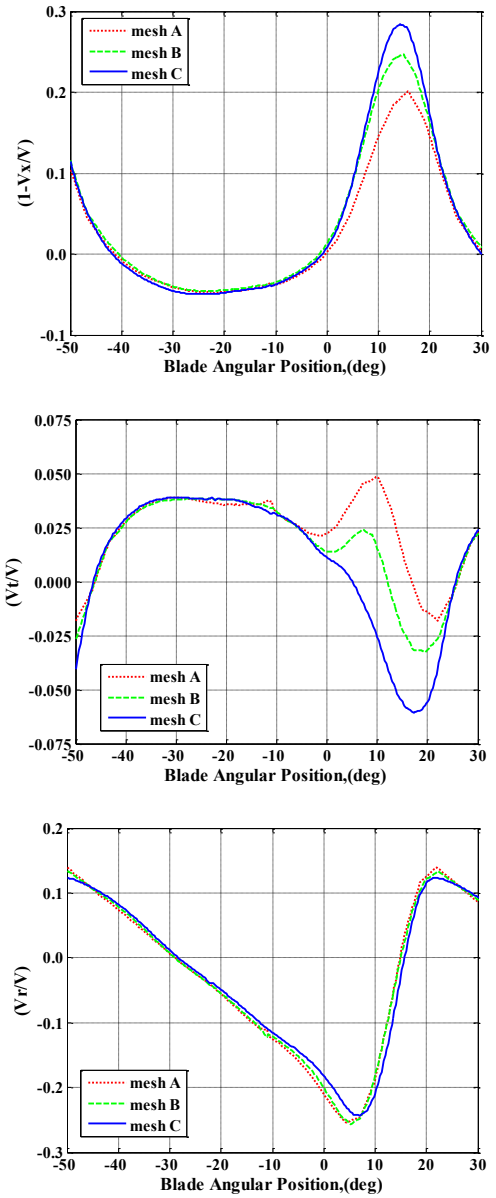

Figure 8: Velocity profiles computed in a plane x/D=0.2 downstream of the propeller mid plane at r/R=1.

From Figures 7 and 8 it is possible to recognize the effect of the mesh resolution on the velocity profiles.

4.4 Cavitation

In order to evaluate the influence of the cavitating behaviour on the propeller performances, we compared the results of the non-cavitating and cavitating flow at three different values of the advance coefficient (J=1.016, 1.269, 1.408). In particular, for the cavitating flow regime we considered the following operational conditions: (J=1.016, σ_n=2.024), (J=1.269, σ_n=1.424), (J=1.408, σ_n=2.00). Following the instructions kindly provided by the Workshop's organizers, we had to adjust, in order to achieve the similar K_T value obtained in the experiment, only the smaller J value, i.e. from 1.019 to 1.016, with the other two J values unchanged.

All the simulations were carried out on mesh B using three different mass transfer models. In Table 2 and 3 the predicted values of the thrust coefficients for the non cavitating and cavitating flow regimes are collected.

Table 2: Thrust coefficients for the non cavitating case

J	$K_{T, NUM}$	$K_{T, EXP}$
1.016	0.382	0.387
1.269	0.240	0.245
1.408	0.166	0.167

In Table 2, the experimental $K_{T,EXP}$ at the smallest advance coefficient J, corresponds, for the reasons given before, to a J value of 1.019.

Table 3: Thrust coefficients for the cavitating flow regimes computed using different mass transfer models.

J	σ_n	$K_{T, NUM}$		
		Zwart	FCM	Kunz
1.016	2.024	0.373	0.374	0.375
1.269	1.424	0.196	0.203	0.210
1.408	2.000	0.133	0.130	0.133

From the results collected in Table 2 it is possible to point out that for the non cavitating conditions the predicted values of the thrust differed less than 2% from the experimental ones. Table 3 shows that the propeller's cavitating performances predicted with the three different mass transfer models were in line with each other. The major differences were observed for (J=1.269, σ_n=1.424). Moreover comparing the result of Table 2 and Table 3 it is possible to notice how, for all the operational conditions, considered in this study, cavitation affected negatively, in a significant way, the propeller's thrust.

In the following in Figure 9 we compare for (J=1.016, σ_n=2.024) the cavitation patterns obtained using the three different mass transfer models. From Figure 9 it is possible to see how the patterns obtained with different models were in line with each other. However it is interesting to notice how Kunz model predicted a cavitation phenomenon with a higher vapour content, and a more sharp water-vapour interface, compared to the other models.

Finally in Figure 10 we show the cavitation patterns for all the operational points, of the present study, predicted using the Zwart model.

CONCLUSIONS

In this work we numerically analyzed, using the ANSYS-CFX 12 commercial CFD solver, the non cavitating and cavitating flow around the PPTC model scale propeller. Simulations were carried out following the experimental setups and for the numerical prediction of the propeller's cavitation behavior three different mass transfer models were used. The cavitation patterns predicted with the different mass transfer models were in line with each other.

Finally, we would like to mention that at the moment work is in progress, within our group, in order to numerically investigate the present problem using the OpenFOAM's C++ CFD libraries.

AKNOWLEDGEMENTS

This work was performed in the context of the project *OpenSHIP*, supported by Regione FVG – POR FESR 2007 – 2013 Obiettivo competitività regionale e occupazione.

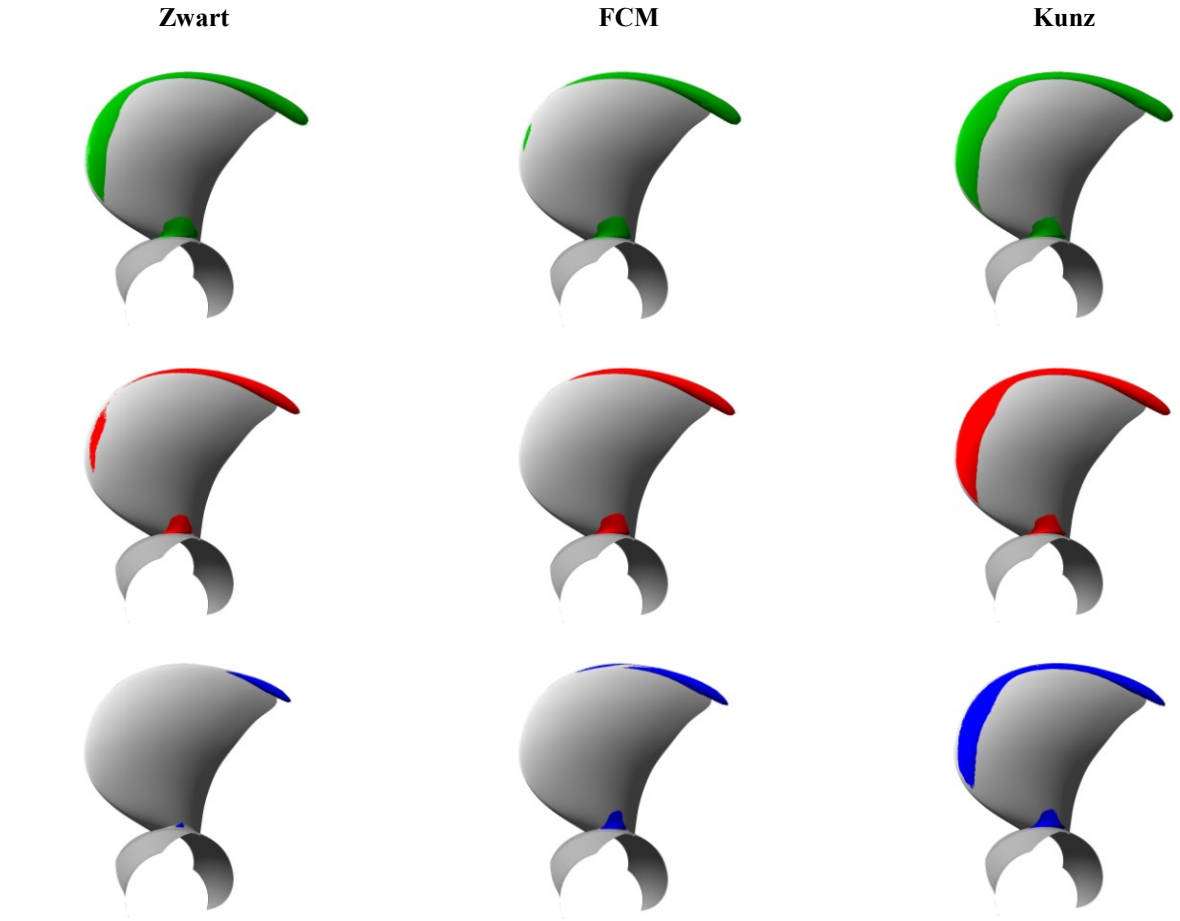

Figure 9: Cavitation patterns predicted for J=1.016, σ_n=2.024 using different mass transfer models. For each model the cavitation pattern is depicted using three different iso-surfaces of the vapour volume fraction α; α=0.20 (green), α=0.50 (red), α=0.80 (blue).

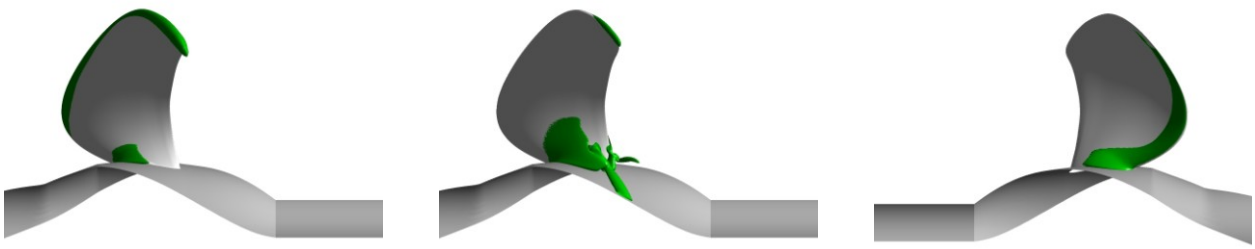

J=1.016, σ_n=2.024 **J=1.269, σ_n=1.424** **J=1.408, σ_n=2.00**

Figure 10: Cavitation patterns depicted as isosurfaces of vapour volume fraction α=0.20 obtained using the Zwart model.

REFERENCES

ANSYS (2010) 'ICEM CFD User Guide', Rel. 12

Kunz, R. F..,Boger, D. A., Stinebring, D. R., Chyczewski, T. S., Lindau, J. W., Gibeling, H. J., Venkateswaran, S., & Govindan, T.R. (2000). 'A preconditioned Navier-Stokes method for two-phase flows with application to cavitation prediction'. Computers and Fluids **29**(8), p.p. 849 – 875.

Menter, F. R. (1998). 'Two-Equation Eddy-Viscosity Turbulence Models for Engineering Applications', AIAA Journal, **32**(8), p.p. 1598-1605.

Morgut, M. & Nobile E. (2011). 'Influence of the mass transfer model on the numerical prediction of the cavitating flow around a marine propeller'. Second International Symposium on Marine Propulsors, smp'11, Hamburg, Germany.

Morgut, M., Nobile E. & Biluš I. (2010). 'Comparison of mass transfer models for the numerical prediction of sheet cavitation around a hydrofoil'. In Press: Int. Journal of Multiphase Flow.

Müller, S.-B., Abdel-Maksoud, M. & Hilbert, G. (2009). 'Scale effects on propellers for large container vessels.' The First International Symposium on Marine Propulsors, smp'09, Trondheim, Norway

Singhal, A. K., Athavale, M. M., Li, H. & Jiang, Y. (2002). 'Mathematical Basis and Validation of the Full Cavitation Model'. Journal of Fluids Engineering **124**, p.p. 617 – 624.

Zwart, P., Gerber, A. G. & Belamri, T. (2004).'A Two-Phase Model for Predicting Cavitation Dynamics'. ICMF 2004 International Conference on Multiphase Flow, Yokohama, Japan.